Available online at www.sciencedirect.com
SCIENCE DIRECT®
Journal of Solid State Chemistry 177 (2004) 2285–2294
JOURNAL OF SOLID STATE CHEMISTRY
http://elsevier.com/locate/jssc

Water-soluble poly(2-(3thienyloxy)ethanesulfonic acid)/V_2O_5 nanocomposites: synthesis and electrochromic properties

Chun-Guey Wu* and Ming-Hau Chung

Department of Chemistry, National Central University, Chung-Li, Taiwan 32054, ROC

Received 2 September 2003; received in revised form 10 November 2003; accepted 23 November 2003

Dedicated to Professor Kwang-Ting Liu on the occasion of his 65th birthday

Abstract

Water-soluble conducting poly(2-(3thienyloxy)ethanesulfonic acid) (PTOESA)/V_2O_5 nanocomposite, $(PTOESA)_xV_2O_5$, was prepared by simply mixing PTOESA with V_2O_5 wet gel at room temperature. XRD data showed that the interlayer spacings of $(PTOESA)_xV_2O_5$ films are 14.0 ± 1.5 Å and increased as the polymer content increased. These values are consistent with the insertion of polythiophene chains into the V_2O_5 layer gallery. The formation of alternative layers of PTOESA and V_2O_5 was further supported by depth profile SIMS analyses. Cyclic voltammograms of $(PTOESA)_xV_2O_5$ film showed two pairs of redox peaks with colors varying from orange, yellowish green, green, to purple blue, depending on the stoichiometry of the nanocomposites. Moreover, a synergetic effect was observed on the electrochromic properties of these nanocomposites. It was found that the optical contrast (ΔOD) of the composites is better than those of PTOESA and V_2O_5 at the film thickness from 150 to 500 nm. The oxidation optical response time of $(PTOESA)_xV_2O_5$ is independent of the stoichiometry and falls in between those of PTOESA and V_2O_5. At higher polymer content ($x > 0.5$), the reduction optical response time of $(PTOESA)_xV_2O_5$ is smaller than those of PTOESA and V_2O_5. Variable temperature conductivity data showed that the conductivity of $(PTOESA)_xV_2O_5$ films increased as temperature increased, characteristic of thermal activated behavior, which was dominated by the interparticle contact resistance. The room-temperature conductivity of water-soluble $(PTOESA)_xV_2O_5$ films was in between those of PTOESA and V_2O_5 xerogel and higher conductivity was found in the composite with lower polymer content. The anomalous conductivity of $(PTOESA)_xV_2O_5$ with high PTOESA content may be due to the reason that the higher the polymer content, the bigger the grain size of $(PTOESA)_xV_2O_5$ film as revealed with scanning electron microscopy and AFM micrographs.

Keywords: Water-soluble; Polythiophenes; V_2O_5; Nanocomposites

1. Introduction

The concept of hybridizing the properties of organic and inorganic materials to form a unique material (with the properties not just the sum of the individual contributions) is an old, well-known strategy [1]. Recently, numerous new applications in the field of material science are related to matter with high surface-to-volume ratio [2]. Therefore, the combination of inorganic and organic components at a nanometer-sized level to a single material has remarkable implications in the development of multifunctional materials. They are innovative materials with promising applications in the field of optics, electronics, ionics, and others [3]. The technological realizations for such advanced materials are expected in the field of 1D and 2D conductivity, membranes, anisotropic optical properties, and non-linear optics [4]. Several approaches to the production of such structures have been described, such as insertion of organic molecules or polymers in anisotropic inorganic network [5–7]; Using organic molecules, or self-assembled aggregate as structure-direction agents to assemble the hybrid structure [8]; and other methods [9]. Significant achievements in the preparation of nano-composites were accomplished in the last few decades [10]. Hybrid method appears as a creative strategy for obtaining new materials with novel properties.

Conducting polymer/V_2O_5 nanocomposites had been synthesized and well studied by Kanatzidis and others

*Corresponding author. Fax: 011886-3-422-7664.
E-mail address: t610002@cc.ncu.edu.tw (C-G. Wu).

0022-4596/$ - see front matter © 2003 Elsevier Inc. All rights reserved.
doi:10.1016/j.jssc.2003.11.036

[3,5a,7a,11]. They were prepared by in situ polymerization/intercalation of monomers in V_2O_5 xerogel. Recently, we had reported [12] the synthesis and characterization of water-soluble conducting polyaniline/V_2O_5 nanocomposite by simply mixing poly(aniline-co-*N*-(4-sulfophenyl)aniline) (PAPSA) aqueous solution with V_2O_5 wet gel. It is an effortless synthesis process with exactly controlled stoichiometry. In this article, we present the synthesis and characterization of another type of water-soluble conducting polymer/V_2O_5 nanocomposites: poly(2-(3thienyloxy)ethanesulfonic acid) (PTOESA)/V_2O_5. Furthermore, PTOESA and V_2O_5 xerogel are both electrochromic materials [13] with rich electrochemical properties. The huge interface interactions between PTOESA and V_2O_5 may create new electrochemical properties, which may not exist in organic polymer or V_2O_5 xerogel. We study the detailed electrochemical properties of $(PTOESA)_xV_2O_5$ nanocomposites. A synergetic effect leading to improved electrochromic properties is emphasized.

2. Experimental section

2.1. Materials

3-Bromothiophene, sodium methoxide, toluene, diethyl ether, *N*-methyl-pyrrolidone, BrC_2H_4OH, $NaHSO_4$, MeOH, HCl(aq), $FeCl_3$, $NaVO_3$ and Dowex-50 × 2-100 resin were purchased from commercial resources and used as received.

2.2. Preparation of water-soluble polythiophene, poly(2-(3thienyloxy)ethanesulfonic acid) (PTOESA)

PTOESA was synthesized by reported methods [14] and the product was identified with IR and UV/Vis/NIR spectroscopy.

2.3. Preparation of V_2O_5 xerogel

V_2O_5 xerogel was synthesized according to a literature report [15]. A HVO_3 aqueous solution was obtained by dissolving 4.0 g of $NaVO_3$ in 250 mL water, then passing the $NaVO_3$ solution through a H^+ ion exchange column packed with 30 g of Dowex-50 × 2-100 resin. Upon standing (for about a week), the HVO_3 aqueous solution spontaneously polymerized to a red V_2O_5 gel via a sol–gel process. The V_2O_5 gel was poured in pitch dishes and allowed the water to evaporate at room temperature automatically. After evaporation of excess water, a dry gel (named xerogel) with a chemical formula of $V_2O_5 \cdot nH_2O$ was formed (the water content depends on the humidity of the environment).

2.4. Preparation of water-soluble poly(2-(3thienyloxy)ethanesulfonic acid–V_2O_5 composites, $(PTOESA)_xV_2O_5$

In a typical reaction, a known amount of aqueous solution of water-soluble PTOESA was mixed well with V_2O_5 wet gel (the concentration of PTOESA and V_2O_5 was determined with UV/Vis absorption intensity based on the absorption–concentration calibration curve). The mixture was then centrifuged to remove the trace amount of insoluble residue. The clear solution was then casted on glass or silicon substrates. The excess water evaporated and a flexible conducting nanocomposite film, which can be peeled off as a free-standing film, was formed on the substrate. The colors of the films are orange, green-yellow, or blue, depending on the mole ratio of PTOESA and V_2O_5. The stoichiometry of the composites was determined by elemental analysis and TGA studies.

2.5. Physicochemical measurements

Fourier transform infrared (FTIR) spectra were recorded as films on Si substrates using a Bio-Rad 155 FTIR spectrometer. UV/Vis/NIR spectra were obtained using Varian Cary 5E spectrophotometer in the laboratory atmosphere at room temperature. Scanning electron microscopy (SEM) and energy dispersive spectroscopy (EDS) studies were done with Hitachi S-800 at 15 kV. Transmission electron micrograph (TEM) was taken with JEOL JEM-2000FXII at the acceleration voltage of 160 kV. X-ray powder diffraction studies were carried out with a Shimadzu XRD-6000 X-ray diffractometer using Cu$K\alpha$ radiation at 30 kV and 30 mA. Depth profile secondary ion mass spectra (SIMS) were done with a Cameca IMS-4f SIMS spectrometer. Thermogravimetric analysis (TGA) was performed with a Perkin-Elmer TGA-7 thermal analysis system using dry nitrogen (or oxygen) as a carrier gas at a flow rate of 100 mL/s. The TGA experiments were conducted from 25°C to 900°C with a linear heating rate of 5°C/min. A Heraeus CHN-O-S Rapid-F002 system was used for elemental analysis.

2.6. Electrochemical studies

For the electrochemical measurement, the composite films (150–500 nm) were deposited on homemade ITO electrodes to be the working electrodes. Electrochemistry was performed in single-compartment, three-electrode cell with a Pt coil counter electrode and an Ag/AgCl reference electrode. The supporting electrolyte was 0.1 M $LiClO_4$ in acetonitrile. The cyclic voltammograms and chronoamperometric analysis were recorded using a Model 263 electrochemical instrument of EG&G PAR potentiostat/galvanostat with a scan rate of

50 mV/S. The absorption spectra of the composites under various applied potentials were in situ recorded with an UV/Vis spectrometer. The electrochromic optical contrast of the nanocomposite films was noted by recording the UV/Vis spectra in the oxidized and reduced states at applied potentials of 1.0 and −0.8 V (vs Ag/Ag^+), respectively. The optical contrast (ΔOD) was estimated by taking the log value of the ratio of the transmittance in the two cases at the wavelength between 400 and 700 nm. The electrical and optical responses were obtained by submitting the nanocomposite films (on ITO electrode) to double potential steps ($E_1 = 1.0$ V, 45 s and $E_2 = -0.8$ V, 45 s); the redox currents and UV/Vis spectra were recorded simultaneously. The electrical oxidation (or reduction) response time (τ_E) was defined as the time needed to reach the 75% of the total oxidation (or reduction) current within 45 s. The optical response time (τ_o) is defined as the time needed to reach 75% of the maximum transmittance change within 45 s.

2.7. Charge transport measurements

The conductivity as a function of temperature was measured using the constant-current, four-probe method. Silver paste was applied to make the electrical contacts. A Keithley 238 programmable electrometer was used to provide a constant current from the two outer probes and to measure the voltage drop between the two inner probes. The floating potential across two inner electrodes was measured to determine the conductivity [16].

3. Results and discussion

3.1. Synthesis and characterization of water-soluble poly(2-(3thienyloxy)ethanesulfonic acid–V_2O_5 composites, $(PTOESA)_xV_2O_5$

When the aqueous solution of PTOESA was mixed with V_2O_5 wet gel, a suspension solution was formed, no observable precipitate was found. To insure the purity of the composite, the suspension solution was centrifuged to remove trace amounts of the insoluble paste. The clear solution was then cast on the glass substrates; the excess water evaporated and dry films were obtained. X-ray diffraction patterns of water-soluble $(PTOESA)_xV_2O_5$ with various stoichiometries (obtained from elemental analysis and/or thermogravimetric analysis) are shown in Fig. 1 and the interlayer spacing and domain size are listed in Table 1. It was found that the *d*-spacings of $(PTOESA)_xV_2O_5$ are 14.0 ± 1.5 Å and increased as polymer content increased. The variation of the *d*-spacings may be because the polymer chains are not located in an orderly fashion on the interlayer gallery of V_2O_5, at least, not as ordered as in the $PAPSA/V_2O_5$ [12] and $PANI/V_2O_5$ [5a] systems. Nevertheless, PTOESA chains do insert in the layer gallery of V_2O_5. Depth profile SIMS analysis showed that the atomic ratios of S and V were very similar through the whole film (see Fig. 2). This shows that the mixing between PTOESA and V_2O_5 was in the nanometer-sized scale and $(PTOESA)_xV_2O_5$ can be considered as a nanocomposite. The stoichiometries of the nanocomposites obtained from elemental analysis and TGA (Fig. 3)

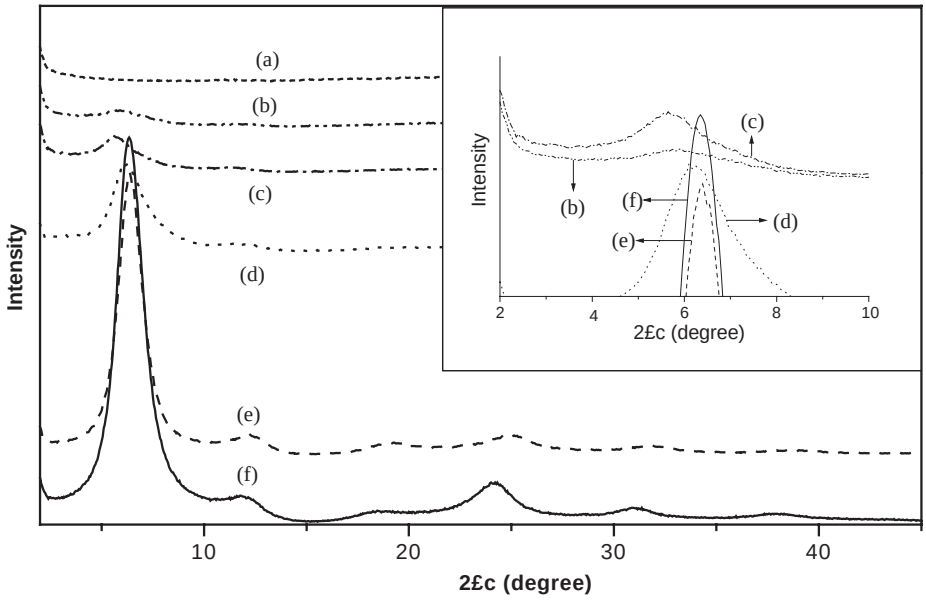

Fig. 1. X-ray diffraction patterns of: (a) PTOESA, (b) $(PTOESA)_{2.11}V_2O_5$, (c) $(PTOESA)_{1.49}V_2O_5$, (d) $(PTOESA)_{0.56}V_2O_5$, (e) $(PTOESA)_{0.07}V_2O_5$, and (f) V_2O_5.

Table 1
The layer spacing and domain size of $(PTOESA)_xV_2O_5$

Sample	*d* spacing (nm)	Crystalline domain size (nm)	Water content (%)
V_2O_5	1.28±0.05	16.6±1.0	8±2
$(PTOESA)_{0.07}V_2O_5$	1.18±0.05	11.9±0.9	8±2
$(PTOESA)_{0.1}V_2O_5$	1.25	8.1	8±2
$(PTOESA)_{0.17}V_2O_5$	1.23±0.16	13.3±1.3	8±2
$(PTOESA)_{0.36}V_2O_5$	1.30±0.1	10.8±0.6	8±2
$(PTOESA)_{0.5}V_2O_5$	1.31±0.02	8.6±0.3	8±2
$(PTOESA)_{0.77}V_2O_5$	1.39	9.1	8±2
$(PTOESA)_{0.96}V_2O_5$	1.49	11.4	8±2
$(PTOESA)_{1.49}V_2O_5$	1.52	10.6	8±2

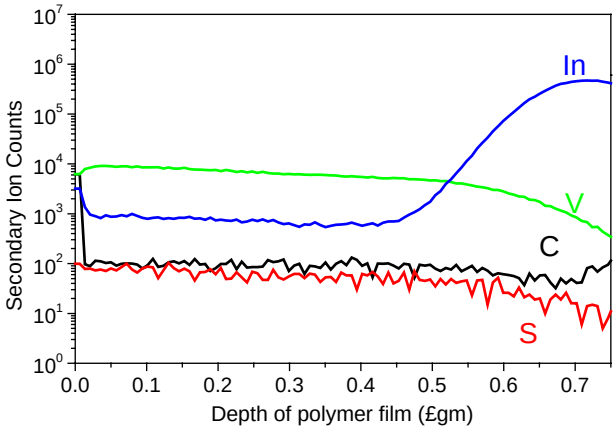

Fig. 2. SIMS of $(PTOESA)_{0.56}V_2O_5$.

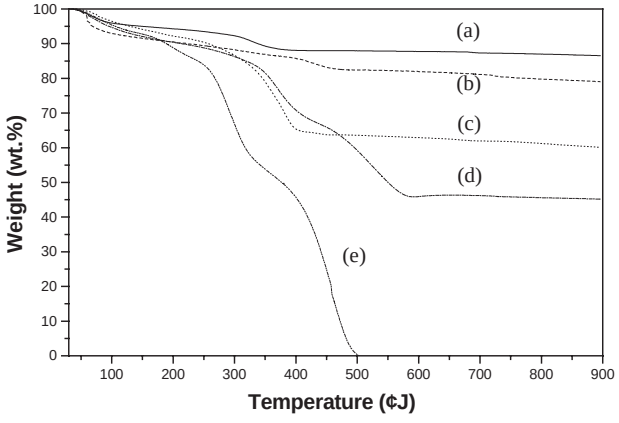

Fig. 3. Thermogravimetric curves of: (a) V_2O_5, (b) $(PTOESA)_{0.07}V_2O_5$, (c) $(PTOESA)_{0.36}V_2O_5$, (d) $(PTOESA)_{0.77}V_2O_5$, and (e) PTOESA.

were very close to those in the reacting mixtures. This result indicated that there is no volatile product formed during the formation of the PTOESA–V_2O_5 nanocomposites.

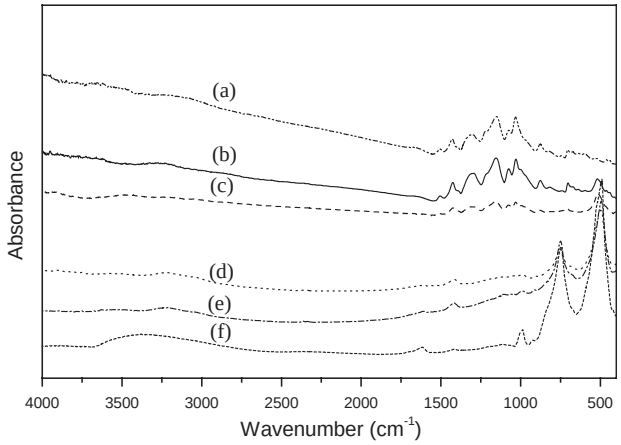

Fig. 4. Infrared spectra of: (a) PTOESA, (b) $(PTOESA)_{0.77}V_2O_5$, (c) $(PTOESA)_{0.36}V_2O_5$, (d) $(PTOESA)_{0.21}V_2O_5$, (e) $(PTOESA)_{0.07}V_2O_5$, and (f) V_2O_5.

3.2. *Physicochemical properties of water-soluble $(PTOESA)_xV_2O_5$ nanocomposites*

IR spectra of water-soluble $(PTOESA)_xV_2O_5$ films are shown in Fig. 4. In low polymer content ($x<0.4$), composites have three peaks at 1012, 750 and 495 cm^{-1}, which are the vibrations of V–O and V=O bond in V_2O_5, indicating that the framework of V_2O_5 is intact when the composite was formed. The absorption peaks at 1430, 1304, 1150, 1030 and 876 cm^{-1}, which belong to PTOESA, did not change. IR data suggest that there is no redox reaction between PTOESA and V_2O_5. TGA (Fig. 3) of $(PTOESA)_{0.5}V_2O_5$ and its individual components show that the thermal stability of the PTOESA in $(PTOESA)_{0.5}V_2O_5$ is better than free polymer. The TGA data suggest that PTOESA chains are intercalated in a thermally stable host.

SEM micrographs of PTOESA, $(PTOESA)_{0.36}V_2O_5$ and V_2O_5 films are shown in Fig. 5. The surface of PTOESA is very smooth, just like a typical organic polymer film. On the other hand, the surface of V_2O_5 film is rather rough, due to the curving of the V_2O_5 sheets during the evaporation of the water molecules. The surface of $(PTOESA)_{0.36}V_2O_5$ (which is smoother than that of V_2O_5 xerogel) reveals a homogeneous morphology; no phase separation is observed. The SEM data showed that by forming the composite with polymer, the surface of V_2O_5 xerogel film was flattened. Water-soluble PTOESA not only flattens the surface of V_2O_5 xerogel but also enhances the dispersion of V_2O_5 sheets as exhibited with TEM micrographs (see Fig. 6). Under TEM microscope, the morphology of $(PTOESA)_xV_2O_5$ with low polymer content ($x = 0.07$) is similar to that of V_2O_5 but has a sparser aggregation and EDS analysis showed that every pieces of $(PTOESA)_xV_2O_5$ slabs contain both V_2O_5 and PTOESA. Interestingly, when the polymer content in $(PTOESA)_xV_2O_5$

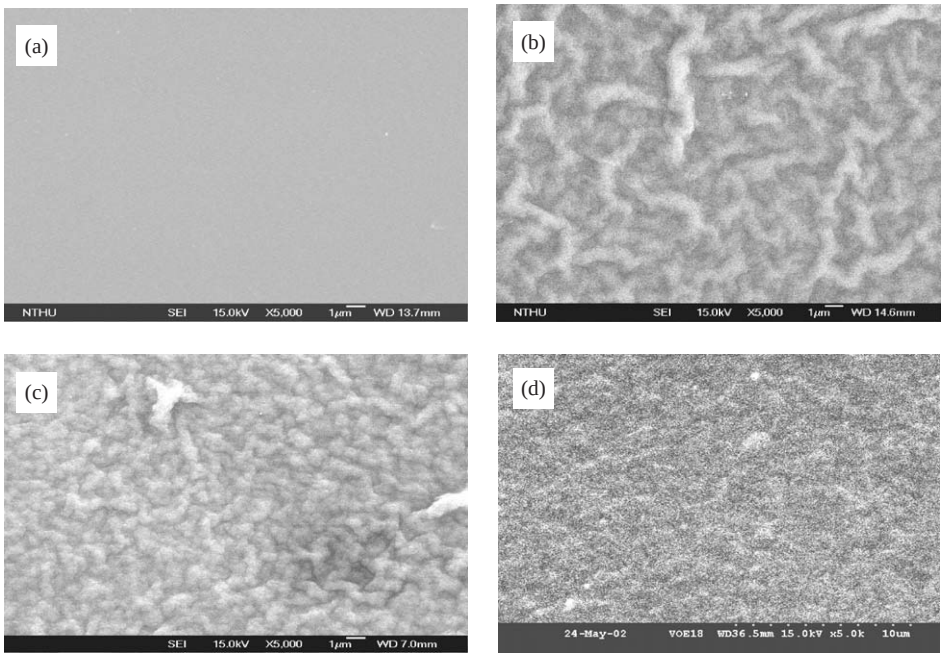

Fig. 5. SEM micrographs of: (a) PTOESA, (b) V_2O_5, (c) $(PTOESA)_{0.56}V_2O_5$, and (d) $(PTOESA)_{0.96}V_2O_5$.

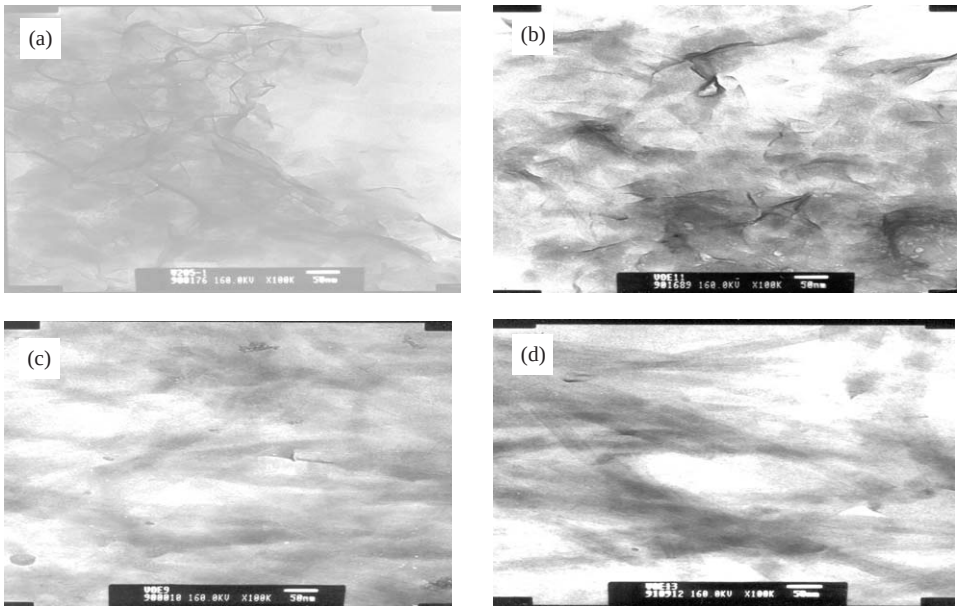

Fig. 6. TEM micrographs of: (a) V_2O_5, (b) $(PTOESA)_{0.07}V_2O_5$, (c) $(PTOESA)_{0.36}V_2O_5$, and (d) $(PTOESA)_{0.56}V_2O_5$ (magnification: 100,000).

increased, wire-like morphology appears. Instead of the thin film morphology observed in V_2O_5, $(PTOESA)_{0.56}V_2O_5$ showed a thin-plate profile with the width of ca. 20 nm and the length longer than 500 nm. Since the samples for TEM viewing were prepared by dipping the copper grid into the aqueous solutions of $(PTOESA)_xV_2O_5$. TEM data suggested that, in the solution, V_2O_5 and PTOESA already wound around with each other to form composite with thin-plate morphology. In other words, $(PTOESA)_xV_2O_5$ is not a co-precipitate of V_2O_5 and PTOESA, there are some interactions between V_2O_5 and PTOESA and the $(PTOESA)_xV_2O_5$ was formed before the film was deposited. Laser scattering particle size analysis showed that the particle size of the $(PTOESA)_xV_2O_5$ in aqueous solution is bigger than that of PTOESA and V_2O_5. This result further supports that $(PTOESA)_xV_2O_5$ plates are formed when PTOESA and V_2O_5 are mixed in the aqueous solution.

The interaction between $(PTOESA)_xV_2O_5$ plates is very weak; therefore, the composite plates pack randomly when the solvent evaporated. The resulting $(PTOESA)_xV_2O_5$ film can be regarded as a film formed

by piling up haphazard small grains of $(PTOESA)_xV_2O_5$ nanocomposite. Consequently, the surface morphology of the nanocomposite film is smoother compared to V_2O_5 film which was formed by drying the stacked hydrated V_2O_5 sheets. The detailed studies of the structure and formation mechanism of $(PTOESA)_xV_2O_5$ nanocomposite will be reported elsewhere. Furthermore, in solution, the interaction (hydrogen bonding or coordination interaction) between PTOESA chain and V_2O_5 sheet is stronger than that between V_2O_5 sheets (van der Waal force). PTOESA chains react with the exfoliated V_2O_5 to form nanometer-sized $(PTOESA)_xV_2O_5$ nanocomposite. Therefore, the electrochemical and charge transport properties of $(PTOESA)_xV_2O_5$ nanocomposite may give a cue to the understanding of V_2O_5 xerogel with nanometer domain.

3.3. The electrochemical properties of $(PTOESA)_xV_2O_5$ nanocomposites

3.3.1. The redox properties

Typical cyclic voltammograms of PTOESA, V_2O_5 and their nanocomposite, $(PTOESA)_xV_2O_5$ are shown in Fig. 7. Two oxidation peaks and two reduction peaks were found in the nanocomposite with the color switches from dark blue to yellow-green to orange at the potential scanned from 1.0 to –1.2 V (vs. Ag/Ag^+). On the other hand, there are two redox pairs for V_2O_5 and only one redox pair of PTOESA at the same potential range. The redox potentials of $(PTOESA)_xV_2O_5$ nanocomposites with different stoichiometry as well as V_2O_5 and PTOESA are listed in Table 2. It was found that V_2O_5 dominated the electrochemical properties of the $(PTOESA)_xV_2O_5$, even when the mole ratio of PTOESA to V_2O_5 is up to 2.11. Nevertheless, the first oxidation potential and the second reduction potential of the $(PTOESA)_xV_2O_5$ film are less negative compared to those of V_2O_5. In other words, $(PTOESA)_xV_2O_5$ nanocomposite is more difficult to oxidize than the pristine V_2O_5. In $(PTOESA)_xV_2O_5$, the electron transfer between V_2O_5 layers is believed to be hindered by PTOESA chains, which have a higher oxidation potential. This reasoning was further supported by the fact that the redox potentials of $(PTOESA)_{0.07}V_2O_5$ are very similar to those of V_2O_5 xerogel.

3.3.2. The electrochromic properties of $(PTOESA)_xV_2O_5$ nanocomposites

There are two important parameters (beside the variation of the colors) for determining the performance of an electrochromic material: one is optical contrast (ΔOD), another is response time (τ). Two types of response times (electrical and optical response times) are discussed in this article. The optical contrast and response time are determined by redox currents or optical transmittances of the samples as stated in the experimental section.

3.3.2.1. The optical contrast (ΔOD) of $(PTOESA)_xV_2O_5$ nanocomposites. The UV/Vis spectra of V_2O_5, PTOESA and $(PTOESA)_xV_2O_5$ films (ca. 250 nm) under various applied potentials are shown in Fig. 8. It was found that all materials have the highest transmittance at a potential of 1.0 V and the lowest transmittance at a potential of –0.8 V and for each sample, its transmittance between 500 and 700 nm is similar. It is obvious

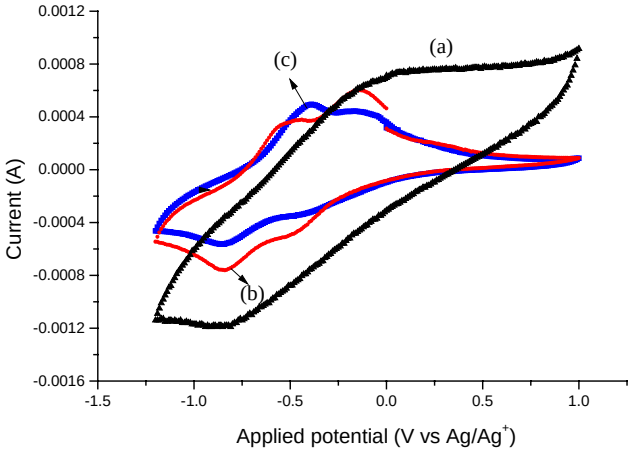

Fig. 7. Cyclic voltammograms of: (a) PTOESA, (b) $(PTOESA)_{0.36}V_2O_5$, and (c) V_2O_5.

Table 2
The redox potentials of V_2O_5, PTOESA, and $(PTOESA)_xV_2O_5$ nanocomposite with different stoichiometry

Sample	First oxidation potential (V vs. Ag/Ag^+)	Second oxidation potential (V vs. Ag/Ag^+)	First reduction potential (V vs. Ag/Ag^+)	Second reduction potential (V vs. Ag/Ag^+)
V_2O_5	−0.44	−0.14	−0.84	−0.52
PTOESA	0.12	—	−0.85	—
$(PTOESA)_{0.07}V_2O_5$	−0.43	−0.14	−0.93	−0.5
$(PTOESA)_{0.36}V_2O_5$	−0.39	−0.16	−0.86	−0.46
$(PTOESA)_{0.56}V_2O_5$	−0.4	−0.13	−0.86	−0.44
$(PTOESA)_{0.96}V_2O_5$	−0.33	−0.13	−0.86	−0.39
$(PTOESA)_{1.49}V_2O_5$	−0.37	−0.19	−0.85	−0.4
$(PTOESA)_{2.11}V_2O_5$.	−0.36	−0.16	−0.84	−0.36

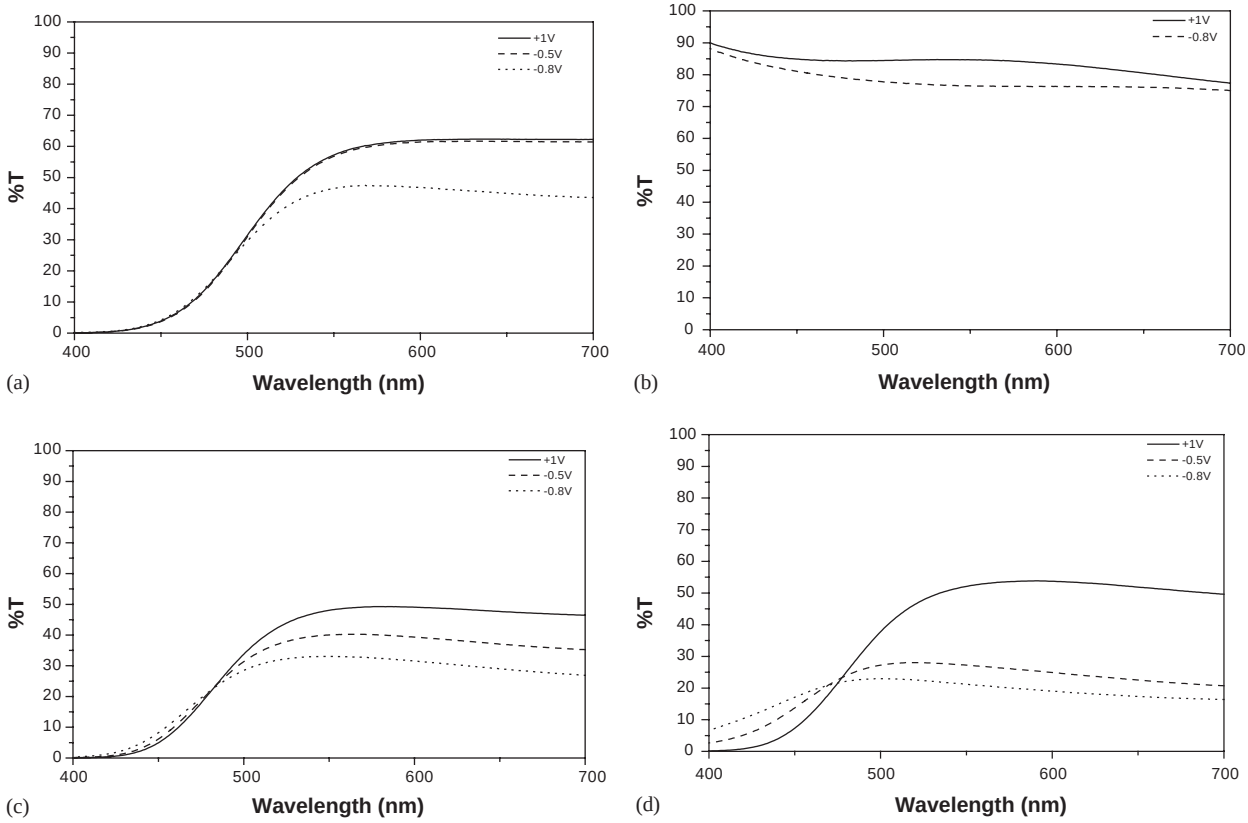

Fig. 8. UV/Vis spectra of: (a) V_2O_5, (b) PTOESA, (c) $(PTOESA)_{0.56}V_2O_5$, and (d) $(PTOESA)_{0.96}V_2O_5$ films at various potentials.

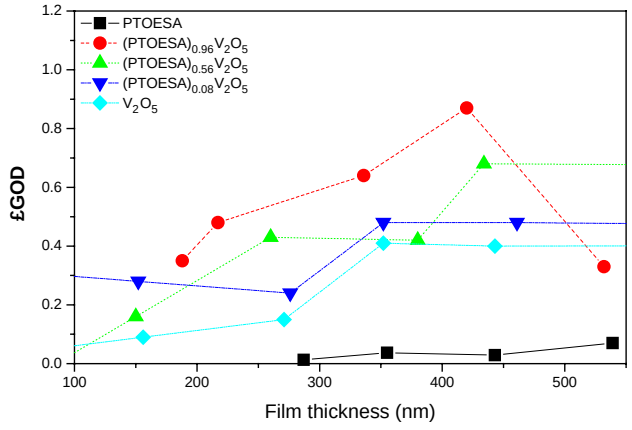

Fig. 9. Variation of ΔOD with the film thickness of PTOESA, V_2O_5, and $(PTOESA)_xV_2O_5$.

that the difference in transmittance (between −0.8 and 1.0 V) for $(PTOESA)_xV_2O_5$ is bigger than those of PTOESA and V_2O_5. Therefore, the ΔOD values of $(PTOESA)_xV_2O_5$ are higher compared to those of PTOESA and V_2O_5 at all wavelengths measured. Interestingly, although the ΔOD of PTOESA films is very small (∼0), $(PTOESA)_xV_2O_5$ with higher PTOESA content has a larger ΔOD value. It was proved that the electrochemical properties of $(PTOESA)_xV_2O_5$ nanocomposites are dominated by V_2O_5 and the function of PTOESA is regarded as a conducting filler or dispersion agent for V_2O_5. V_2O_5 in $(PTOESA)_xV_2O_5$ with higher content of PTOESA has a better dispersion. These results suggest that V_2O_5 in the nanometer domain size has a better optical performance compared to bulk state.

The optical contrast (ΔOD) depends also on the thickness of $(PTOESA)_xV_2O_5$ films. In general, the thicker (up to 400 nm) the nanocomposite film, the higher the ΔOD value. When the thickness of the nanocomposite film is lager than 400 nm, the ΔOD value decreased again. This is because the redox reactions of $(PTOESA)_{0.56}V_2O_5$ are controlled by kinetics. Thick $(PTOESA)_{0.56}V_2O_5$ film cannot be totally oxidized (or reduced) at short (1 second) potential application time. The variation of ΔOD (at 700 nm) with film thickness[1] is different between $(PTOESA)_xV_2O_5$, PTOESA and V_2O_5 as shown in Fig. 9. It was found that the ΔOD of all sample films increased as the film thickness increased. When the film thickness is less than 400 nm, the ΔOD values of $(PTOESA)_xV_2O_5$ nanocomposites are higher than those of PTOESA and V_2O_5. All $(PTOESA)_xV_2O_5$ films (except thin film with very low PTOESA content)

[1] The thickness of (PTOESA)xV2O5 composite films was calculated form the calibration curve of thickness vs. the absorption intensity of UU/Vis spectra. The thickness of the films was measured from the SEM images of the film.

have ΔOD exceeding 0.3, which is the threshold value for application in electrochromic devices. The elevated ΔOD was due to the synergetic effect of two electrochromic materials. The electrochromic stability of $(PTOESA)_xV_2O_5$ films is probed by the variation of ΔOD values with the reduction–oxidation cycles, as shown in Fig. 10. It was found that the ΔOD stabilizes after 5 redox cycles and keep pretty much the same values up to 50 redox cycles. Furthermore, in general, the electrochromic stability of $(PTOESA)_xV_2O_5$ is better than PTOESA and V_2O_5. The formation of the nanocomposites did offer a great possibility for synthesis of new materials with enhanced properties, such as the electrochromic property. The results demonstrated here give a good qualitative, and to a certain degree quantitative, information that may be of valuable help in designing electrochromic devices with specific tailor-made optical properties.

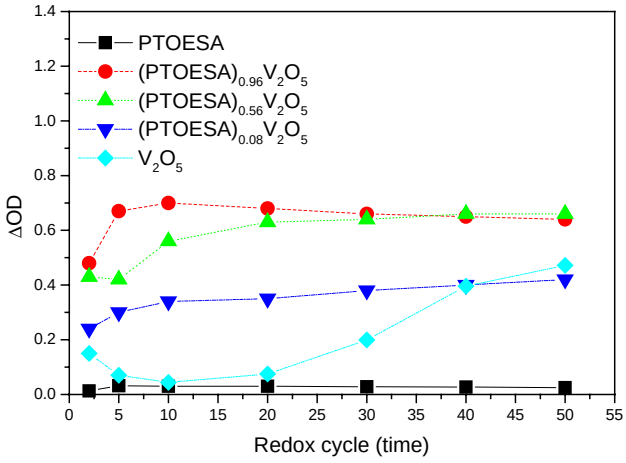

Fig. 10. Variation of ΔOD with the redox cycle number of PTOESA, V_2O_5, and $(PTOESA)_xV_2O_5$ (film thickness ~250 nm).

3.3.2.2. The electrical and optical response times of $(PTOESA)_xV_2O_5$ nanocomposites. The response times in electrochromic device are governed by the diffusion of charge compensating of counterions through the thin films during redox switching. Generally, the counterions have a high degree of mobility attributable to an open framework [17]. Composites with the less dense

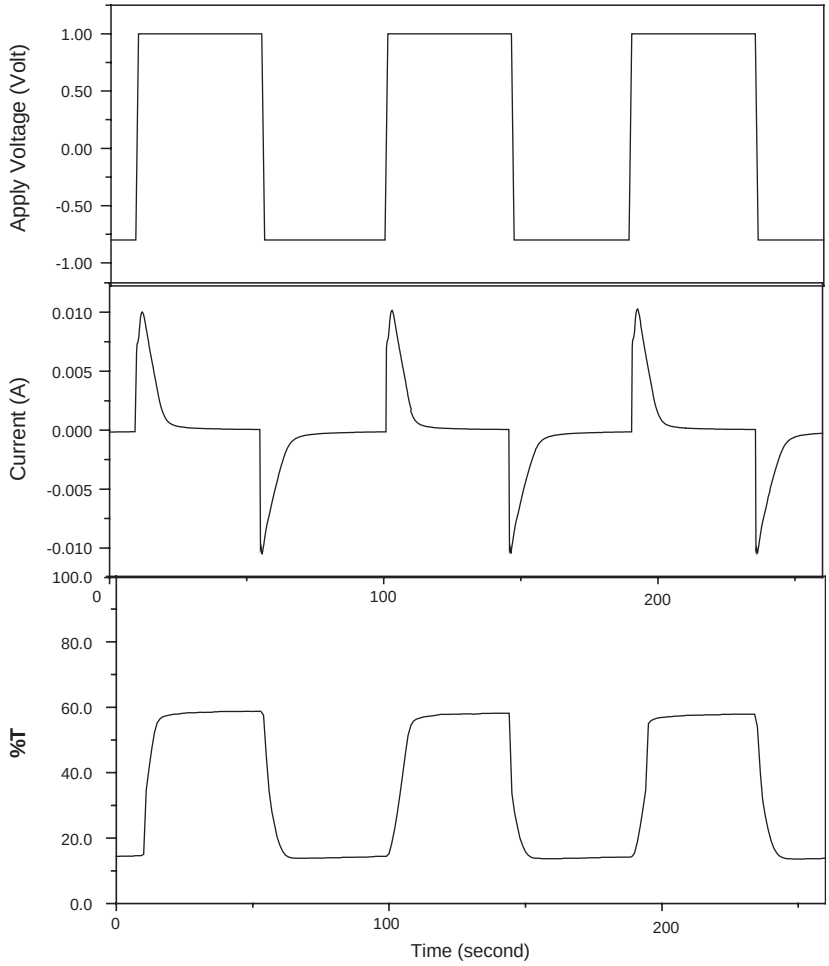

Fig. 11. (a) Electrical, and (b) optical responses for coloring and bleaching of $(PTOESA)_{0.56}V_2O_5$ when submitted to double potential steps.

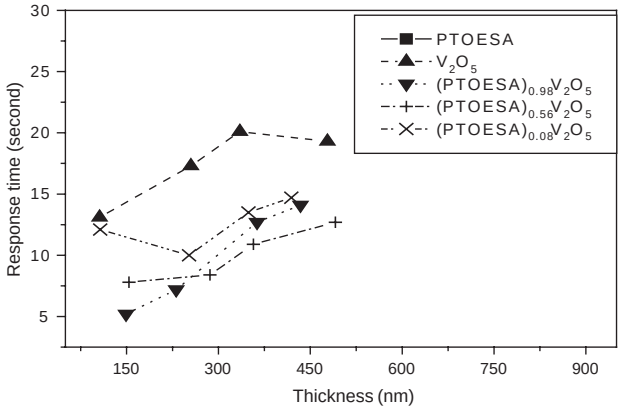

Fig. 12. Electrical response time vs. thickness of PTOESA, V_2O_5, and $(PTOESA)_xV_2O_5$.

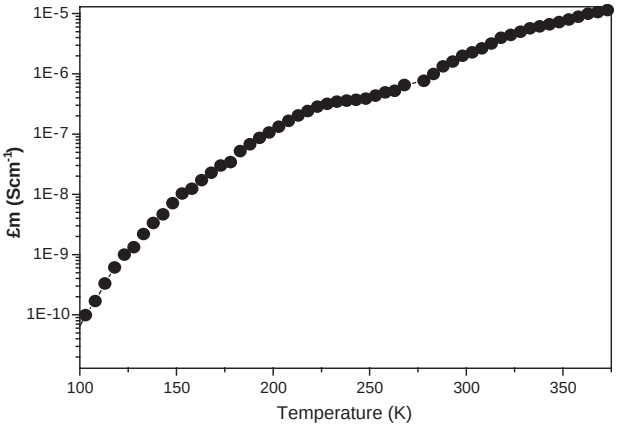

Fig. 13. Variable temperature conductivity of $(PTOESA)_{0.36}V_2O_5$.

Table 3
The optical response times (τ_o, s) for PTOESA, V_2O_5 and $(PTOESA)_xV_2O_5$ with various thicknesses

Sample	Thickness (Å)							
	1500		2500		3500		4500	
	Ox.[a]	Red.[b]	Ox.	Red.	Ox.	Red.	Ox.	Red.
V_2O_5 xerogel	4	1	8	3	9	6	14	5
PTOESA	—	—	3	7	7	7	9	9
$(PTOESA)_{0.98}V_2O_5$	3	3	6	4	8	3	14	5
$(PTOESA)_{0.56}V_2O_5$	2	2	6	4	8	5	11	5
$(PTOESA)_{0.08}V_2O_5$	1	1	6	4	8	3	12	4

[a] Ox.: oxidation.
[b] Red.: reduction

structure may thereby lead to shorter electrochemical response time of the device. Typical electrical and optical responses for coloring and bleaching of $(PTOESA)_xV_2O_5$ when submitted to double potential steps are shown in Fig. 11 The current did not change with the number of double potential steps indicating that $(PTOESA)_xV_2O_5$ has good electrochemical reversibility. The electrical response times (τ_e) also depend on the film thickness as shown in Fig. 12. $(PTOESA)_xV_2O_5$ has shorter reduction electrical response time compared to its individual components PTOESA and V_2O_5. τ_e of $(PTOESA)_xV_2O_5$ decreased as PTOESA content increased. We attribute this trend to the possibility that the $(PTOESA)_xV_2O_5$ has a higher intrinsic conductivity compared to V_2O_5. The conductivity of PTOESA, V_2O_5, and $(PTOESA)_xV_2O_5$ will be discussed in the next paragraph. The optical response times (τ_o) for PTOESA, V_2O_5 and $(PTOESA)_xV_2O_5$ with various thickness are listed in Table 3. It was found that for thin $(PTOESA)_xV_2O_5$ films, τ_o falls between those of PTOESA and V_2O_5. Nevertheless, the reduction optical response times of $(PTOESA)_xV_2O_5$ are shorter than those of its individual components PTOESA and V_2O_5 when the films thickness is greater than 250 nm. The improved response time is also due to the synergetic effect between two electroactive materials. The detailed studies on the electrochemical kinetics of these nanocomposites and their individual components will be reported elsewhere. Furthermore, V_2O_5 xerogel is flexible in the oxidized form but very brittle in the reduced state. On the other hand, the conjugated polymer is ductile at neutral state and becomes rigid when oxidized. Nevertheless, $(PTOESA)_xV_2O_5$ films have good mechanical property both in the oxidized and reduced forms: another synergetic effect.

3.4. The charge transport properties of $(PTOESA)_xV_2O_5$ nanocomposites

PTOESA and V_2O_5 xerogel are both conducting materials. The major charge carriers of $(PTOESA)_xV_2O_5$ films could be either polarons associated with $d^1(V^{4+})$ centers found on the V_2O_5 lattice or bipolarons located on the PTOESA backbone. Therefore, the charge transport properties of $(PTOESA)_xV_2O_5$ will depend on the mobility of these two types of carriers. Variable temperature conductivity of $(PTOESA)_{0.36}V_2O_5$ film is shown in Fig. 13. The conductivity increased with increasing temperature, characteristic of thermal activated behavior, which is due to interparticle contact resistance. This behavior was also observed in polythiophenes [14] and V_2O_5 xerogel [15]. The room conductivity of $(PTOESA)_xV_2O_5$ films is in between PTOESA and V_2O_5 films and increased as the polymer content decreased (see Table 4). We may expect that the conductivity of $(PTOESA)_xV_2O_5$ film with higher PTOESA content will be better, since PTOESA has a higher conductivity compared to V_2O_5. However, the continuity and surface roughness (see the SEM micrographs shown in Fig. 5) of $(PTOESA)_xV_2O_5$ with high polymer content are not as good as $(PTOESA)_xV_2O_5$ with low PTOESA content (the surface roughness of $(PTOESA)_{0.56}V_2O_5$ and $(PTOESA)_{0.08}V_2O_5$, obtained

Table 4
Room-temperature conductivity and activation energy of PTOESA, V_2O_5 and $(PTOESA)_xV_2O_5$

Sample	Conductivity (S/cm)	Activation energy (eV)
V_2O_5	5.7×10^{-9}	0.036
$(P3TOESH)_{0.08}V_2O_5$	2.9×10^{-6}	0.037
$(P3TOESH)_{0.4}V_2O_5$	2×10^{-6}	0.036
$(P3TOESH)_{0.96}V_2O_5$	8.4×10^{-7}	0.039
P3TOESH	3.1×10^{-4}	0.008

from the AFM studies, are 5.04 and 2.98 nm, respectively). Therefore, the lower conductivity of $(PTOESA)_xV_2O_5$ film with higher PTOESA content is not an intrinsic property. It is due to the fact that $(PTOESA)_xV_2O_5$ with higher polymer content has less smooth surface; consequently, has a higher particle contact resistance (higher activation energy), therefore shows lower conductivity.

4. Conclusions

This article reports the blending of aqueous solutions of organic polymer, PTOESA, and inorganic metal oxide, V_2O_5, into organic/inorganic nanocomposite. Electron microscopic data revealed that the nanocomposite was formed via self-assembly of polymer chains and exfoliated V_2O_5 sheets in aqueous solution. The synergetic effect of two electrochromic materials increased the optical contrast; reduced the optical and electric response times; improved the mechanical strength. The design of hybrid nanocomposites seeks to get the best out of two individual components with complementary strengths to form materials with improved properties. This work has demonstrated that the benefits accrued by having nanometer-scale materials interact with the second phase can go beyond increasing the mechanical strength and thermal or chemical stability toward improving the optical properties.

Acknowledgments

Financial support from the National Science Council of the Republic of China (NCS 91-2113-M-008-019) is gratefully acknowledged.

References

[1] (a) C. Sanchez, G.J. Soler-Illia, F. Ribot, T. Lalot, C.R. Mayer, V. Cabuil, Chem. Mater. 13 (2001) 3061–3083;
(b) A.K. Cheetham, et al. (Eds.), Better Ceramics Through Chemistry VI, Materials Research Society Symposium Proceedings 346 (1994);
(c) U. Schubert, N. Husing, A. Lorenz, Chem. Mater. 7 (1995) 2010.
(d) P. Gomez-Romero, Adv. Mater. 13 (2001) 163–174.
[2] K. Rajeshwar, N.R. Tacconi, C.R. Chenthamarakshan, Chem. Mater. 13 (2001) 2765–2782.
[3] D.A. Loy, K.J. Shea, Chem. Rev. 95 (1995) 1431.
[4] P. Judeinstein, C. Sanchez, J. Mater. Chem. 6 (1996) 511–525.
[5] (a) M.G. Kanatzidis, C.-G. Wu, H.O. Marcy, C.R. Kannewurf, J. Am. Chem. Soc. 111 (1989) 4139–4141.
(b) M.G. Kanatzidis, C.-G. Wu, H.O. Marcy, D.C. DeGroot, C.R. Kannewurf, A. Kostikas, V. Papaefthymiou, Adv. Mater. 2 (1990) 364–366.
[6] (a) P. Brandt, R.D. Fisher, E.S. Martinez, R.D. Calleja, Angew. Chem. Int. Ed. Engl. 28 (1989) 1265–1266.
(b) P. Enzel, T. Bein, Phys. Chem. 93 (1989) 6270–6272.
(c) J.V. Caspar, V.D. Ramamurthy, R. Corbin, J. Am. Chem. Soc. 113 (1991) 600–610.
(d) C.-G. Wu, T. Bein, Science 266 (1994) 1013–1015.
[7] (a) C.-G. Wu, D.C. DeGroot, H.O. Marcy, J.L. Schindler, C.R. Kannewurf, Y.J. Liu, W. Hirpo, M.G. Kanatzidis, Chem. Mater. 8 (1996) 1992–2004.
(b) H. Inoue, H. Yoneyama, J. Electroanal. Chem. 233 (1987) 291–294.
[8] (a) S. Baral, P. Schoen, Chem. Mater. 5 (1993) 14.
(b) A. Firouzi, D. Kumar, L.M. Bull, T. Besier, P. Sieger, Q. Huo, S.A. Walker, J.A. Zasadzinski, C. Glinka, J. Nicol, D. Margolese, G.D. Stucky, B.F. Chmelka, Science 267 (1995) 1138.
[9] M.W. Weimer, H. Chen, E.P. Giannelis, D.Y. Sogah, J. Am. Chem. Soc. 121 (1999) 1615–1616.
[10] (a) L.L. Klein (Ed.), Hybrid Organic–Inorganic Materials, Sanchez Special Issue of J. Sol–Gel Sci. Technol. 5 (1995);
(b) L.L. Klein, C. Noyes (Ed.), Sol–Gel Technology for Thin Film, Fiber, Preforms, Electronics and Specialty Shapes, Park Ridge, NJ, 1988.
(c) H. Schmidt, in: D.R. Uhlmann, D.R. Ulrich (Eds.), Ultrastructure Processing of Advanced Materials, Wiley, New York, 1992 (Chapter 38);
(d) J.E. Mark, C.Y.-C. Lee, P.A. Bianconi (Eds.), Hybrid Organic–Inorganic Composites, ACS Symposium Series, Washington, DC, Vol. 585, 1995.
[11] (a) C.-G. Wu, M.G. Kanatzidis, H.O. Marcy, C.R. Kannewurf, D.C. Degroot, Polym. Mater. Sci. Eng. 61 (1989) 969–973.
(b) C.-G. Wu, H.O. Marcy, D.C. Degroot, C.R. Kannewurf, M.G. Kanatzidis, Mater. Res. Soc. Symp. Proc. 173 (1990) 317–322.
(c) M. Lira-Cant, P. Gomez-Romero, J. Solid State Chem. 147 (1999) 601–608.
[12] (a) C.-G. Wu, C.Y. Hwang, J. Mater. Chem. 11 (2001) 2061–2066.
(b) C.-G. Wu, S.S. Hsu, J.Y. Hwang, M.H. Chung, J. Chin. Chem. Soc. 49 (2002) 907–914.
[13] (a) A.G. MacDiarmid, W. Zheng, NRS Bulletin 24–29 (1997);
(b) J. Gustafsson, O. Inganas, A. Andersson, Synth. Met. 62 (1991) 17.
[14] (a) G. Zotti, M.C. Gallazzi, G. Zerbi, S.V. Meille, Synth. Met. 73 (1995) 217–225.
(b) M. Chayer, K. Faid, M. Leclarc, Chem. Mater. 9 (1997) 2902–2905.
[15] J. Lemerle, L. Nejem, J. Lefebvre, J. Inorg. Nucl. Chem. 42 (1980) 17–20.
[16] F. M. Smiths, Bell System Tech. J. (1958) 710–718.
[17] S.A. Sapp, G.A. Sotzing, J.R. Reynolds, Chem. Mater. 10 (1998) 2101–2108.